Biogeochemical evidence of anaerobic methane oxidation on active submarine mud volcanoes on the continental slope of the Canadian Beaufort Sea

Dong-Hun Lee[1], Jung-Hyun Kim[2,*], Yung Mi Lee[2], Alina Stadnitskaia[3], Young Keun Jin[2], Helge Niemann[4,5], Young-Gyun Kim[6], Kyung-Hoon Shin[1,**]

[1]Hanyang University ERICA campus, 55 Hanyangdaehak-ro, Sangnok-gu, Ansan-si, Gyeonggi-do 426-791, South Korea

[2]KOPRI Korea Polar Research Institute, 26 Songdomirae-ro, Yeonsu-gu, Incheon 21990, South Korea

[3]European Council for Maritime Applied R&D, Rue Marie de Bourgogne 52-54, B-1000 Bruxelles, Belgium

[4]NIOZ Royal Netherlands Institute for Sea Research, Department of Marine Microbiology and Biogeochemistry, NL1790 AB Den Burg, Texel, The Netherlands

[5]CAGE - Centre for Arctic Gas Hydrate, Environment and Climate, Department of Geology, UiT The Arctic University of Norway, 9037 Tromsø, Norway

[6]Research Institute for Earth Resources, Kangwon National University, 24341, Chuncheon, South Korea

[*]Corresponding author:
Tel.: +82 32 760 5377
jhkim123@kopri.re.kr

[**]Corresponding author:
Tel.: +82 31 400 5536
shinkh@hanyang.ac.kr

Abstract

In this study, we report lipid biomarker patterns and phylogenetic identities of key microbial communities mediating anaerobic oxidation of methane (AOM) in active mud volcanoes (MVs) on the continental slope of the Canadian Beaufort Sea. The carbon isotopic compositions ($\delta^{13}C$) of *sn*-2- and *sn*-3-hydroxyarchaeol showed the highly ^{13}C-depleted values (–114 ‰ to –82 ‰) associated with a steep depletion in sulfate concentrations within 0.7 m of sediment depths. This suggested the presence of methanotrophic archaea involved in sulfate dependent–AOM, albeit in a small amount. The ratio of *sn*-2-hydroxyarchaeol to archaeol (>1) and operational taxonomic units (OTUs) indicated that archaea of the ANME-2c and ANME-3 clades were involved in AOM. Higher $\delta^{13}C$ values of archaeol and biphytanes (BPs) (–55.2 ± 10.0 ‰ and –39.3 ± 13.0 ‰, respectively) suggested that archaeal communities were also assimilating AOM-derived inorganic carbon. Furthermore, the distinct distribution patterns of methanotrophs in the three MVs appears to be associated with varying intensities of ascending gas fluids. Consequently, our results suggest that the niche diversification of active mud volcanoes has shaped distinct archaeal communities that play important roles in AOM in the Beaufort Sea.

Keywords: Arctic, Beaufort Sea, submarine mud volcano, methane, anaerobic oxidation of methane (AOM), lipid biomarkers, 16S rRNA

1 Introduction

Mud volcanoes (MVs) are kilometer-scale, low-temperature, seepage-related geomorphological features that provide some of the most remarkable indications of fluid venting (Ivanov et al., 1998). The roots of MVs can reach depths of up to 20 km (Shnukov et al., 2005); thus they provide key information about the geological history of the area and its possible hydrocarbon potential (Ivanov et al.,1992, 1998). Comprehensive investigations of numerous on- and off-shore MV provinces have revealed the overwhelming input of hydrocarbon gases in their formation. Eruptions often manifest as a catastrophic emission of fluids consisting of hydrocarbon gases (especially methane), hydrogen sulfide, carbon dioxide, petroleum products, water, and a complex mixture of sediments, so-called "mud breccia" (Akhmanov,1996; Akhmanov and Woodside, 1998; Ivanov et al.,1998). The occurrence of active MVs could constitute a significant portion of the geological sources of global atmospheric methane emissions (Kopf, 2002; Milkov et al., 2003). In the Arctic Ocean, where the temperature of the bottom water has been increasing (Levitus et al., 2000; Westbrook et al., 2009; Polyakov et al., 2010), concern has been raised that the warming water will cause the disintegration of sediment-bound methane gas hydrates (Marín-Moreno et al., 2016). That would lead to higher methane concentrations/fluxes in surface sediments and thus the ascending methane would quickly be released into the water column and potentially the atmosphere (Niemann et al., 2006; Felden et al., 2010). The submarine MVs is therefore of considerable interest in global warming scenarios, since methane is a greenhouse gas that is >20 times more potent than carbon dioxide (Wuebbles and Hayhoe, 2002; Etminan et al., 2016). Accordingly, MV sediments can be regarded as a model system for studying the biogeochemical dynamics of sediments characterized by high methane fluxes.

Across the Canadian Beaufort continental slope, active MVs were discovered at water depths of ~282 m, ~420 m, and ~740 m during the multibeam bathymetric mapping surveys

conducted in 2009 and 2010 (Campbell et al., 2009). They were named with respect to their water depths, i.e., MV282, MV420, and MV740 (Blasco et al., 2013; Saint-Ange et al., 2014). Previous investigations based on sediment coring and mapping with an autonomous underwater vehicle (AUV) and a remotely operated vehicle (ROV) showed that these MVs are young and active edifices characterized by ongoing eruptions (Paull et al., 2015). The gas ascending via these MVs consists of >95 % methane with $\delta^{13}C_{CH4}$ values of –64 ‰ (Paull et al., 2015), indicating a microbial methane source (Whiticar, 1999). Siboglinid tubeworms and white bacteria mats were reported at MV420 (Paull et al., 2015). Those organisms typically consume sulfide and are thus often associated with elevated anaerobic methanotrophy in near-surface sediments because sulfide is one end product of the anaerobic oxidation of methane (AOM), with sulphate as the terminal electron acceptor (Boetius and Wenzhöfer, 2013; Paull et al., 2015). AOM is mediated by several clades of anaerobic methanotrophic archaea (ANME) that typically form syntrophic associations with sulphate-reducing partner bacteria (Knittel and Boetius, 2009):

$$CH_4 + SO_4^{2-} \rightarrow HCO_3^- + HS^- + H_2O$$

A powerful tool to investigate AOM communities in sediments is the analysis of membrane lipids combined with their compound-specific carbon isotopic composition ($\delta^{13}C$), which can be used to chemotaxonomically infer community composition (Niemann and Elvert, 2008 and references therein). In particular, low $\delta^{13}C$ values in AOM-derived lipids are widely used to trace AOM in ancient (e.g. Zhang et al., 2003; Stadnitskaia et al.,2008a,b; Himmler et al., 2015) and modern seep settings (e.g. Hinrichs and Boetius, 2002; Niemann et al., 2005; Chevalier et al., 2011, 2014). Although the ebullition of methane from the Beaufort Sea MVs has been documented before (Paull et al., 2015), the sediment methane dynamics, including the role of

AOM as a barrier against uprising methane in these systems, has not been investigated.

In this study, we thus investigated three sediment cores recovered from active MVs on the continental slope of the Canadian Beaufort Sea during the ARA05C expedition with the R/V ARAON in 2014. By using a combination suite of lipid and nucleic acid analyses with bulk geochemical parameters, our study sheds light on the specific archaeal communities involved in AOM at active MVs in the Canadian Beaufort Sea.

2 Material and Methods

2.1 Sample collection

Three sediment cores were recovered using a gravity corer during the ARA05C expedition of the South Korean icebreaker R/V ARAON in the Canadian Beaufort Sea in August 2014 (Fig. 1A-C). Core ARA05C-10-GC (70°38.992'N, 135°56.811'W, 282 m water depth, 221 cm core length), core ARA05C-01-GC (70°47.342'N, 135°33.952'W, 420 m water depth, 272 cm core length), and core ARA05C-18-GC (70°48.082'N, 136°05.932'W, 740 m water depth, 300 cm core length) were retrieved from the active MV sites MV282, MV420 and MV740, respectively. Upon recovery, all sediment cores showed active degassing (Fig. 1D). When the sediment cores were split, we observed a mousse-like texture in cores ARA05C-10-GC and ARA05C-01-GC, related to outgassing as a result of the pressure change during recovery. Gas hydrates in the shape of about ≤2 cm thick isolated veins were observed at the bottom (230 to 300 cm) of core ARA05C-18-GC. The split sediment cores were lithologically described, and then subsampled for total organic carbon (TOC), lipid biomarkers and 16S rRNA gene sequences on board. After subsampling, sediment samples were stored at –20°C for geochemical analyses and at –80°C for microbial analyses.

2.2 Bulk geochemical analysis

Sediment samples were freeze-dried and homogenized using an agate mortar prior to the TOC analyses. Sediment samples (~1 g) were then treated with 8 mL 1N HCl to remove carbonates before measuring the TOC content and its isotopic composition using an elemental analyzer (EuroEA3028, Eurovector, Milan, Italy) connected to an isotope ratio mass spectrometer (Isoprime, GV Instruments, Manchester, UK). All isotope ratios of TOC are reported using the δ-notation (per mil) with respect to the Vienna Pee Dee Belemnite (VPDB). The analytical errors (standard deviations of repeated measurements of the internal standard IAEA CH_6) were smaller than ±0.1 wt.% for TOC, and ±0.1 ‰ for $\delta^{13}C_{TOC}$.

2.3 Lipid extraction and purification

The homogenized sediment samples (ca. 10 g) were extracted with an accelerated solvent extractor (Dionex ASE 200, Dionex Corporation, Sunnyvale, CA) using a solvent mixture of 9:1 (v:v) dichloromethane (DCM) to methanol (MeOH) at a temperature of 100°C and a pressure of 7.6×10^6 Pa. The total lipid extract was dried over anhydrous Na_2SO_4 and was treated with tetrabutylammonium sulfite reagent to remove elemental sulfur. An aliquot was chromatographically separated into apolar and polar fractions over an Al_2O_3 (activated for 2 h at 150°C) column with solvents of increasing polarity. The apolar fraction was eluted using hexane:DCM (9:1, v:v), and the polar fraction was recovered with DCM:MeOH (1:1, v:v) as eluent. After column separation, 40 µl of 5α-androstane (10 µg/mL) were added to the apolar fraction as an internal standard. The polar fraction was divided into two aliquots, to which either C_{22} 7,16-diol (10 µg/mL) or C_{46} GDGT (10 µg/mL) was added as an internal standard. Half of the polar fraction containing C_{22} 7,16-diol was dried and silylated with 25 µL N,O-bis(trimethylsilyl)trifluoroacetamide (BSTFA) and 25 µL pyridine before heating it to 60°C for 20 min to form trimethylsilyl derivatives. The second half of the polar fraction containing C_{46} GDGT was re-dissolved by sonication (5 min) in hexane:isopropanol (99:1, v:v) and then

148 filtered with a 0.45-µm PTFE filter. Afterwards, an aliquot of the filtered fraction was treated
149 with HI following the procedure described by Kaneko et al. (2011) in order to cleave ether
150 bonds from glycerol dialkyl glycerol tetraethers (GDGTs), thereby releasing biphytanes (BPs)
151 which can be analyzed by a gas chromatography (GC).
152
153 2.4 Identification and quantification of lipid biomarkers
154 All apolar and polar fractions were analyzed using a Shimazu GC (Shimazu Corporation,
155 Kyoto, Japan) equipped with a splitless injector and a flame ionization detector for compound
156 quantification. A fused silica capillary column (CP-sil 5 CB, 25-m length, 0.32-mm i.d., and
157 0.12-µm film thickness) was used with He (1.3 mL/min) as a carrier gas. The samples were
158 injected under constant flow at an initial oven temperature of 70°C. The GC oven temperature
159 was subsequently raised to 130°C at a rate of 20°C/min, and then to 320°C at 4°C/min with a
160 final hold time of 15 min. Concentrations were obtained by comparing the peak area of each
161 compound with that of 5α-androstane for the apolar fraction and C_{22} 7,16-diol for the polar
162 fraction. Compound identifications for the apolar, silylated and BP polar fractions were
163 conducted using a Shimazu GC connected to a GCMS-QP2010 mass spectrometer (MS)
164 operated at 70 eV (cycle time of 0.9 s, resolution of 1000) with a mass range of *m/z* 50–800.
165 The samples were subjected to the same temperature conditions and capillary column described
166 for GC analysis. Molecular structures were determined by comparing their mass spectral
167 fragmentation patterns and retention times with previously published data.
168 An aliquot of the filtered polar fractions was analyzed by high-performance liquid
169 chromatography–atmospheric pressure positive ion chemical ionization–mass spectrometry
170 using an Agilent 6120 Series LC/MSD SL system (Agilent Technologies, Santa Clara, CA)
171 equipped with an auto-injector and Chemstation chromatography manager software.
172 Separation was achieved on two UHPLC silica columns (2.1 × 150 mm, 1.7 µm), fitted with

2.1 × 5 mm pre-columns of the same material and maintained at 30°C. Injection volumes varied from 1 µL. GDGTs were eluted isocratically with 82% A and 18% B for 25 min, followed by a linear gradient to 35% B over 25 min, then to 100% B over 30 min, and finally maintained for 20 min, where A = hexane and B = hexane:2-propanol (90:10, v:v). The flow rate was 0.2 mL/min, with a total run time of 90 min. After each analysis, the column was cleaned by back-flushing hexane:2-propanol (90:10, v:v) at 0.2 mL/min for 20 min. Conditions for APCI-MS were as follows: nebulizer pressure 60 psi, vaporizer temperature 400°C, drying gas (N_2) flow 6 mL/min and temperature 200°C, capillary voltage –3.5 kV, corona 5 µA (~3.2 kV). Detection was achieved in single ion monitoring of $[M + H]^+$ ions (dwell time 35 ms), as described by Schouten et al. (2007). GDGTs were quantified by integrating peak areas and using the internal standard according to Huguet et al. (2006).

2.5 Compound-specific stable carbon isotope analysis

The $\delta^{13}C$ values of selected compounds were determined by GC/combustion/isotope ratio mass spectrometry (GC-C-IRMS), as described by Kim et al. (2017). An IRMS (Isoprime, GV Instruments, UK) was connected with a GC (Hewlett Packard 6890 N series, Agilent Technologies, Santa Clara, CA) via a combustion interface (glass tube packed with copper oxide (CuO), operated at 850°C). The samples were subjected to the same temperature conditions and capillary column described for the GC and GC-MS analyses. Calibration was performed by injecting several pulses of reference gas CO_2 of known $\delta^{13}C$ value at the beginning and the end of each sample run. Isotopic values are expressed as $\delta^{13}C$ values in per mil relative to the Vienna-PeeDee Belemnite (VPDB). The $\delta^{13}C$ values were further corrected using a certified isotope standard (Schimmelmann alkane mixture type A6, Indiana University). The correlation coefficients (r^2) of the known $\delta^{13}C$ values of certified isotope standards with

the average values of the measured samples were higher than 0.99. In the case of silylation of alcohols, we corrected the measured $\delta^{13}C$ values for the isotopic composition of the methyl adducts (the $\delta^{13}C$ value of the BSTFA = –19.3 ± 0.5 ‰). In order to monitor the accuracy of the measurements, standards with known $\delta^{13}C$ values were repeatedly analyzed every 5–6 sample runs. Standard deviations of carbon isotope measurements were generally better than ±0.4 ‰, as determined by repeated injections of the standard.

2.6 Genomic DNA extraction and amplification of 16S rRNA genes

Sediment samples stored at –80°C were freeze-dried, and genomic DNA was extracted from ~0.5 g of freeze-dried samples using the FastDNA Spin Kit for Soil (Q-Biogene, Carlsbad, CA, USA). 16S rRNA gene was amplified by polymerase chain reaction (PCR) using the 8F (3-CTCAGAGTAGTCCGGTTGATCCYGCCGG-5') / 519R (3'-ACAGAGACGAGGTDTTACCGCGGCKGCTG-5') primers with barcodes for archaeal community analysis. PCR was carried out with 30 µL of reaction mixture containing DreamTaq Green PCR Master Mix (2×) (Thermo Fisher Scientific, Waltham, MA, USA), 1 µL of 5 µM primers, and 4 µL of genomic DNA. The PCR procedure included an initial denaturation step at 94°C for 3 min, 30 cycles of amplification (94°C for 1 min, 55°C for 1 min, and 72°C for 1.5 min), and a final extension step at 72°C for 5 min. Each sample was amplified in triplicate and pooled. PCR products were purified using the LaboPass purification kit (Cosmogenetech, Seoul, Korea). Due to PCR failure for samples below 0.6 m in the MV740 sample, these samples were not included in further analysis.

2.7 Archaeal community and phylogenetic analysis

Sequencing of the 16S rRNA amplicon was carried out by Chun Lab (Seoul, South Korea)

using a 454 GS FLX-Titanium sequencing machine (Roche, Branford, CT, USA). Preprocessing and denoising were conducted using PyroTrimmer (Oh et al., 2012). Sequences were processed to remove primer, linker, and barcode sequences. The 3′ ends of sequences with low quality values were trimmed when the average quality score for a 5-bp window size was lower than 20. Sequences with ambiguous nucleotides and those shorter than 250 bp were discarded. Chimeric reads were detected and discarded using the *de novo* chimera detection algorithm of UCHIME (Edgar et al., 2011). Sequence clustering was performed using CLUSTOM (Hwang et al., 2013) with a 97 % similarity cutoff. Taxonomic assignment was conducted for representative sequences of each cluster by EzTaxon-e database search (Kim et al., 2012). Raw reads were submitted to the National Center for Biotechnology Information (NCBI) Sequence Read Archive (SRA) database (accession number PRJNA433786).

For phylogenetic analysis of operational taxonomic units (OTUs) based on 16S rRNA genes, we selected OTUs belonging to the class *Methanomicrobia* that composed more than 1 % of the relative abundance and aligned them with those of *Methanomicrobia* in jPHYDIT. A phylogenetic tree was constructed using the maximum-likelihood algorithm (Felsenstein et al., 1981) with MEGA 6 (Tamura et al., 2013). The robustness of the tree topologies was assessed by bootstrap analyses based on 1,000 replications of the sequences.

3 Results

3.1 Bulk geochemical and microbial lipid analyses

Dissolved sulfate concentrations in sediment cores from MV282, MV420, and MV740 ranged from 0.1 mM to 26.8 mM and sharply decreased within 0.7 m in core depths (Fig. 2, see also Paull et al., 2015). Overall, the TOC contents of core sediments from MV282, MV420 and MV740 ranged from 1.2–1.5 wt.%, 1.0–1.3 wt.%, and 1.1–1.3 wt.%, respectively (Fig. 2, see also Table 1). Similarly, $\delta^{13}C_{TOC}$ values in MV282, MV420 and MV740 cores showed little

246 variation, with average values of –26.3±0.07 ‰, –26.2±0.05 ‰, and –26.3±0.06 ‰,
247 respectively (Fig. 2, see also Table 1).

248 Isoprenoid dialkyl glycerol diethers (DGDs), considered as biomarkers diagnostic for
249 ANMEs such as archaeol (2,3-di-*O*-phytanyl-*sn*-glycerol) and *sn*-2-hydroxyarcaheol (2-*O*-3-
250 hydroxyphytanyl-3-*O*-phytanyl-sn-glycerol), were identified in the polar fractions of all three
251 cores (Fig. S1); their concentrations were 0.03–0.09 μg/g and 0.01–0.13 μg/g, respectively (Fig.
252 3, see also Table 1). *Sn*-3-hydroxyarchaeol was identified only in MV282 and MV420
253 sediments at concentrations of 0.01–0.08 μg/g (Fig. 3, see also Table 1). Among non-isoprenoid
254 DGDs, we identified DGD (If) with *anteiso* pentadecyl moieties attached at both the *sn*-1 and
255 *sn*-2 positions in all three cores. The concentrations of non-isoprenoid DGD (If) ranged from
256 0.06 to 0.25 μg/g (Fig. 3, see also Table 1). Isoprenoid glycerol dialkyl glycerol tetraethers
257 (GDGTs) containing 0 to 3 cyclopentane moieties (GDGT-0 to GDGT-3) and crenarchaeol
258 which, in addition to 4 cyclopentane moieties, contains a cyclohexane moiety, were detected
259 in all samples investigated (Fig. 4). Overall, the isoprenoidal GDGTs were dominated by
260 GDGT-0 and crenarchaeol, with concentrations of 0.02–0.19 μg/g and 0.02–0.25 μg/g,
261 respectively, whereas GDGT-1 and GDGT-2 showed much lower concentrations (≤0.02 μg/g)
262 in the three cores. In the apolar fractions, we did not detect any isoprenoid hydrocarbons that
263 are typically associated with ANMEs, i.e., the C_{20} compound 2,6,11,15-tetramethylhexadecane
264 (crocetane) or the C_{25} compound 2,6,10,15,19-pentamethylicosane (PMI).

265 At the three MVs, the $\delta^{13}C$ values of archaeol and *sn*-2-hydroxyarchaeols ranged from –
266 79.8 to –38.5 ‰ and from –113.9 to –82.1 ‰, respectively (Fig. 3, Table 1). The $\delta^{13}C$ values
267 of *sn*-3-hydroxyarchaeol were as low as –93.1 ‰. The $\delta^{13}C$ values of the non-isoprenoid DGD
268 (If) varied between –46.9 and –31.9 ‰. The $\delta^{13}C$ values of BPs derived from the isoprenoid
269 GDGTs ranged from –63.4 to –16.7 ‰. The $\delta^{13}C$ values of BP-1 (on average –51.0 ‰) were
270 slightly more depleted than those of BP-0 (on average –34.2 ‰), BP-2 (on average –28.3 ‰)

271 and BP-3 (on average –27.5 ‰).

272

273 3.2 Depth profile of archaeal communities

274 Archaeal communities were phylogenetically classified as the taxonomic level of class
275 (Table S1 and Fig. S2). The archaeal classes detected were Miscellaneous Crenarchaeotal
276 Group (MCG)_c, Methanomicrobia, SAGMEGMSBL_c, Thermoplasmata, Lokiarchaeota_c
277 (formerly Marine Benthic Group B), MHVG3_c, Group 1a_c, and Group 1b_c. MCG_c of the
278 phylum Bathyarchaeota was the most dominant archaeal class at the three MVs at a range of
279 depths, with the exception of the surface of MV420, accounting for 39.7 to 99.2 % of the total
280 archaeal sequences. In contrast to the archaeal communities below 0.3 m in MV282 and 1.1 m
281 in MV420, which were dominated by MCG_c, shallow archaeal communities at depths of 0.0–
282 0.2 m at MV282, 0.1–0.7 m at MV420, and 0.1–0.6 m at MV740 had different compositions
283 in the MVs. The class *Methanomicrobia* represented a relatively high proportion (up to 20.9 %)
284 in these shallow depths at all three MVs.

285

286 **4 Discussion**

287 4.1 Signals of AOM activity in Beaufort Sea mud volcanoes

288 Active gas bubble emissions into the overlying water column have previously been
289 observed at all the investigated MVs, i.e., MV282, MV420, and MV740 (Paull et al., 2011 and
290 2015). A sharp decrease in pore water sulfate concentration and a rapid increase in sediment
291 temperature near the seafloor indicates the ascension of sulfate-depleted, warm fluids
292 containing methane from these MVs (Paull et al., 2015). Thus, several lines of evidence suggest
293 that interstitial methane gas is likely saturated near the seafloor of the investigated MVs,
294 meaning that both an electron acceptor (sulfate) and a donor (methane) for AOM are present in
295 the near-surface sediments. Furthermore, an indirect indication of AOM in near-surface

296 sediments is the presence of thiotrophic organisms, i.e., siboglinid tubeworms closely related
297 to *Oligobrachia haakonmosbiensis* and the white bacterial mats found at the summit of MV420
298 (Paull et al., 2015). Such thiotrophs, which consume the AOM end product, sulfide, are
299 typically found in habitats characterized by high AOM activity in the near-surface sediments
300 (Niemann et al., 2006; Rossel et al., 2011; Felden et al., 2014).

301 AOM at active methane seeps typically proceeds with sulfate as the terminal electron
302 acceptor (Boetius et al., 2000, Reeburgh, 2007; Knittel et al., 2009; James et al., 2016),
303 although recent research also found indications for AOM with electron acceptors other than
304 sulfate, i.e. oxidised Mn and Fe species (Beal et al., 2009) or nitrate/nitrite (Haroon et al., 2013).
305 The key microbial communities involved in sulfate-dependent AOM are anaerobic methane
306 oxidisers (ANMEs) in association with sulfate reducing partner bacteria (Knittel et al., 2009),
307 although ANMEs may also mediate sulfate-dependent AOM without bacterial partners
308 (Milcuka et al., 2012). AOM with alternative electron acceptors in marine settings is probably
309 mediated by specialised ANMEs (Beal et al., 2009; Haroon et al., 2013), but it remains unclear
310 how far potential bacterial partners are involved in these processes. At the MVs investigated
311 here, we found indications for sulfate-methane transition zones (SMTZ) because sulfate
312 penetrated only about 0.20 m (MV270), 0.20 m (MV420) and 0.45 m (MV740) into the sea
313 floor, and we found corresponding elevated abundancies of sulfate-dependent AOM
314 communities and their lipid biomarkers (Fig.2 and see discussion on AOM communities in
315 sediments in section 4.2). In contrast to sulfate, the other potential electron acceptors for AOM
316 mentioned above are typically depleted at shallow depths because redox-reactions are more
317 thermodynamically feasible than AOM (Reeburgh, 2007). We did not detect any of the archaeal
318 communities (i.e., *Methanoperedens nitroreducens*, Haroon et al., 2013) that mediate AOM
319 with electron acceptors other than sulfate, which makes alternative modes of AOM at the
320 investigated MVs rather unlikely.

4.2 Contribution of AOM to sedimentary biomass

AOM-derived biomass (including lipids) is generally depleted in ^{13}C compared to the $\delta^{13}C$-values of source methane as a result of isotopic fractionation during methane assimilation (Whiticar, 1999). As AOM-related biomarkers, we found substantial amounts of *sn*-2-hydroxyarchaeol among the isoprenoid DGDs in all three MV sediment cores (Fig. 3). *Sn*-3-hydroxyarchaeol, an isomer of *sn*-2-hydroxyarchaeol (e.g. Pancost et al., 2000; Elvert et al., 2005; Niemann et al., 2005; Bradley et al., 2009), was also detected in MV282 but not in MV420 or MV740, except at 0.7 m in MV420 (Fig. 3). The $\delta^{13}C$ values of *sn*-2-hydroxyarchaeol were more depleted than the $\delta^{13}C_{CH4}$ values (by about –64 ‰, Paull et al., 2015), with average $\Delta\delta^{13}C$ values (lipid-methane) of –35.5 ‰ in MV282, –33.8 ‰ in MV420, and –29.5 ‰ in MV740. Notably, the $\Delta\delta^{13}C$ values of *sn*-2-hydroxyarchaeol were slightly larger in MV282 than in the other MVs. Similar to *sn*-2-hydroxyarchaeol, the $\delta^{13}C$ values of *sn*-3-hydroxyarchaeol in the MV sediments were generally more depleted than the $\delta^{13}C_{CH4}$ values. Accordingly, the depleted-$\delta^{13}C$ values of *sn*-2- and *sn*-3-hydroxyarchaeol indicated recent AOM occurrence in sediment where sulfate was present. On the other hand, the depleted $\delta^{13}C$ values of *sn*-2-hydroxyarchaeol detected below the SMTZ were likely a fossil AOM signature (Lee et al., 2013). Non-isoprenoid DGD (If), identified as a robust marker of sulfate-reducing bacteria (SRB) involved in AOM (e.g. Pancost et al., 2001a; Werne et al., 2002), was detected throughout all three MV sediment cores (Fig. 3). However, the $\delta^{13}C$ values of the non-isoprenoid DGD (If) (–46.9 to –32.6 ‰) were enriched in ^{13}C relative to the ascending methane in the MVs. Therefore, our $\delta^{13}C$ data from the non-isoprenoid DGD (If) suggest that those compounds originate from a mixed community mediating AOM and other processes.

Furthermore, our measurements of the TOC content and $\delta^{13}C_{TOC}$ values in the three sediment cores revealed narrow ranges of 1.2±0.1 wt.% and –26.4±0.6 ‰, respectively (Fig. 2,

346 see also Table 1), without the negative isotopic excursion that has often been observed in MVs
347 in association with methane-derived biomass from AOM (e.g. Haese et al., 2003; Werne et al.,
348 2004). Therefore, in accordance with methane ebullition to water column (Paull et al., 2015),
349 our bulk geochemical data suggest that the contribution of AOM-biomass to sedimentary TOC
350 was rather low at the MVs we investigated, which is in line with our findings that the non-
351 isoprenoid GDGTs substantially originate from bacterial sources unassociated with
352 methanotrophy.

353 Similarly, we found substantial amounts of archaeal lipids that originated from sources
354 other than AOM. All sediment cores from the three MVs showed a predominance of GDGT-0
355 and crenarchaeol (Fig. 4), revealing the contribution of marine pelagic Thaumarchaeota
356 (Schouten et al., 2013). The isoprenoid GDGT distributions also did not show a clear
357 dominance of GDGT-2 over GDGT-0. The values of the GDGT-0/crenarchaeol (Liu et al.,
358 2011), the GDGT-2/crenarchaeol (Weijers et al., 2011), and the methane index (Zhang et al.,
359 2011) were also low, with ranges of 0.8–1.7, 0.1–0.2, and 0.2–0.4, respectively. Thus, the
360 GDGT signals found here indicate the negligible contribution of Euryarchaeota to AOM and
361 the GDGT pool (e.g. Pancost et al., 2001b; Zhang et al., 2003; Niemann et al., 2005;
362 Stadnitskaia et al., 2008a, b). The ^{13}C-enriched isotopic signatures of BPs (Table 1) relative to
363 methane provide further evidence that the isoprenoid GDGTs derived from methanotrophic
364 archaea were low in the investigated sediments. For example, at sites characterized by high
365 AOM activity, previous studies found GDGT-1 and -2 at concentrations of up to 20 µg/g, 100-
366 fold higher than in our results (Stadnitskaia et al., 2008b). We can only speculate about the
367 reasons for the low abundances of AOM-related archaeal communities contributing to the
368 GDGT pool. One possibility is a rather recent onset in seepage activity at the coring sites, which
369 would leave too little time for the slow-growing AOM communities, which are characterized
370 by doubling times on the month scale, to have grown large (Nauhaus et al., 2007).

4.3 AOM-related microbial communities in Beaufort Sea mud volcanoes

4.3.1 Chemotaxonomy

The composition of microbial lipids and their $\delta^{13}C$ values can be used to infer the chemotaxonomic composition of microbes involved in sulfate-dependent AOM (Niemann and Elvert, 2008). Previously, three groups of anaerobic methanotrophic archaea (ANME-1, ANME-2 and ANME-3) have been reported in a diversity of cold seep environments, which are related to methanogens of the orders *Methanosarcinales* and *Methanomicrobiales* (Knittel and Boetius, 2009). Archaeol is ubiquitous in archaea, often serving as an indicator of methanogenic archaea in a wide range of environments including MVs (e.g. De Rosa and Gambacorta, 1988; Koga et al., 1993, 1998; Pancost et al., 2011). In contrast, *sn*-2-hydroxyarchaeol has only been found in certain orders of methanogens such as *Methanosarcinales, Methanococcales*, *Methanopyrales, Thermoplasmatales, Sulfolobales* and *Methanomicrobiales* (e.g. Kushwaha and Kates, 1978; Koga et al., 1993, 1998; Koga and Morii, 2005), and s*n*-3-hydroxyarchaeol has been detected in *Methanosarcinales* (*Methanosaeta concilii*) and *Methanococcales* (*Methanococcus voltae*) (Ferrante et al., 1988; Sprott et al., 1993).

Microbial communities dominated by ANME-2 at the cold seeps of the northwestern Black Sea contained higher amounts of *sn*-2-hydroxyarchaeol relative to archaeol, whereas the reverse was observed in microbial mats dominated by ANME-1 (Blumenberg et al., 2004). Indeed, the ratio of isotopically depleted *sn*-2-hydroxyarchaeol relative to archaeol can be used to distinguish ANME-1 (0–0.8) from ANME-2 (1.1–5.5), with ANME-3 (2.4) falling within the range of ANME-2 (Niemann et al., 2006; Niemann and Elvert, 2008). In our dataset, the concentration of *sn*-2-hydroxyarchaeol was slightly higher than that of archaeol in MV282, but lower in MV420 and MV740 (Fig. 3, see also Table 1). Accordingly, the *sn*-2-

hydroxyarchaeol/archaeol ratio was between 1.3 and 1.8 in MV282, but below 0.7 for most of the samples from MV420 and MV740, except for at depths of 0.7 m (1.4) in MV420 and 0.4–0.6 m (0.9–1.1) in MV740 (Fig. 3, see also Table 1). This observation suggests that ANME-2 (or ANME-3) was involved in AOM in MV282, whereas ANME-1 was probably involved in AOM in MV420 and MV740, except for at the depths mentioned above.

However, the $\delta^{13}C$ values of archaeol were on average –62.6 ‰ in MV282, –49.4 ‰ in MV420, and –54.3 ‰ in MV740, except for at 0.7 m in MV420 (–79.8 ‰). Hence, the $\delta^{13}C$ values of archaeol in most of the MV sediments appeared to be enriched in ^{13}C in comparison to that of the ascending methane in the MVs (about –64 ‰, Paull et al., 2015), indicating admixture from processes other than AOM. Hence, it appears that the ratio of *sn*-2-hydroxyarchaeol to archaeol was generally high in all investigated MVs, hinting a negligible involvement of ANME-1 in AOM even in MV420 and MV740. Previous studies showed that GDGTs were mostly absent in ANME-2-dominated settings, but not in ANME-1-dominated settings, which typically contain substantial amounts of GDGT-1 and GDGT-2 (e.g., Blumenberg et al., 2004; Stadnitskaia et al., 2008a, b; Chevalier et al., 2011; Kaneko et al., 2013). The GDGT distributions found here (Fig. 4) indeed show a clear dominance of GDGT-0 and crenarchaeol over GDGT-1 and GDGT-2. Hence, our lipid data indicate that ANME-2 and/or ANME-3 are involved in AOM in the Beaufort Sea MVs rather than ANME-1. We did not detect crocetane, which is diagnostic for ANME-2 (Elvert et al., 1999), but we also found no PMIs which are structurally similar to crocetane and produced by ANME-1, -2 and -3 (Niemann and Elvert, 2008), so we could not carry out a further chemotraxonomic distinction of the dominant ANME groups.

4.3.2 Nucleic acid based phylogeny

To further identify key AOM communities, we investigated the archaeal community by

pyrosequencing of 16S rRNA genes. In line with geochemical and biomarker signals for AOM in the surface sediments of the investigated MVs, we found archaeal sequences of the *Methanomicrobia*, which contains the order *Methanosarcinales* (i.e., the clade to which the ANME archaea also belong) at higher abundances in the upper depths of the MV sediment cores than the lower depths (see Table S2 and Fig. S2). To further clarify the phylogenetic position within the class *Methanomicrobia* (comprising both methanogens and methanotrophs), phylogenies of the three most dominant (more than 1 % of all archaeal sequences) *Methanomicrobia* OTUs (c116, c1698, and c1784) were inferred from 16S rRNA gene sequences (Supplementary Information Table S2). The OTU c116 represented 2.5–14.1 % and 0.2–6.7 % of the *archaeal* sequences at core depths of 0.0–0.2 m in MV282 and 0.1–1.1 m in MV420, respectively, whereas this OTU was less than 0.2 % at MV740 (Supplementary information Table S2). The OTU c1698 accounted for more than 1 % of the archaeal sequences at the surface of MV282 but was absent at other MVs. The OTU c1784 accounted for 1.2–6.8 % and 3.7–14.9 % of the archaeal sequences at core depths of 0.0–0.2 m in MV282 and 0.4–0.6 m in MV740, respectively. In contrast, this OTU was rarely detected at all depths of MV420, except for at the depth of 0.7 m. The OTUs c116 and c1698 belonged to ANME-3 archaeal lineage and the OUT c1784 formed a cluster with sequences of ANME-2c, a distinct lineage of *Methanosarcinales* (Fig. 5). Hence, the occurrence of these sequences, together with our lipid data, provides evidence that the AOM communities belong to the ANME-2 and ANME-3 clades; ANME-1 does not seem to play a role at the investigated Beaufort Sea MVs. In line with our geochemical and lipid analyses, the abundance of ANME-sequences was also low, underscoring that the contribution of the AOM communities to the archaeal biomass at the MVs investigated here was rather minor. Instead, we found that most archaeal sequences belong to the MCG_c clade (up to 99.2 % of all sequences) within the phylum Bathyarchaeota. Although members of this clade were previously shown to perhaps be involved in methane oxidation in

446 marine and estuary settings (Inagaki et al., 2006; Jiang et al., 2011; Li et al., 2012), little is
447 known about their physiology and biogeochemical roles in nature.
448
449 4.4 Mechanism controlling microbial communities in Beaufort Sea mud volcanoes
450 16S rRNA signatures from the Beaufort Sea MVs revealed the presence of AOM related
451 to archaeal ANME-2 and ANME-3, albeit in relatively low proportions (Fig. 5). The ANME-2
452 can be divided into three subgroups, ANME-2a, ANME-2b, and ANME-2c (e.g. Orphan et al.,
453 2001; Knittel et al., 2005). In the Beaufort Sea MVs, the ANME-2c subgroup was detected
454 (Fig. 5). A previous study at Hydrate Ridge (Cascadia margin off Oregon, USA) showed that
455 ANME-2c was dominant at symbiotic clam *Calyptogena* sites, accounting for >75 % of the
456 total ANME-2, whereas ANME-2a was the most abundant at a site covered by the sulfide-
457 oxidizing bacterium *Beggiatoa*, accounting for up to 80 % (Knittel et al., 2005). Fluid flow
458 rates and the methane fluxes from the seafloor were substantially weaker at *Calyptogena* sites
459 than at *Beggiatoa* sites (e.g. Tryon et al., 1999; Sahling et al., 2002). The distinct distribution
460 of ANME-2 subgroups might reflect their sulfide tolerance and oxygen sensitivity (Roalkvam
461 et al., 2011). It appears that ANME-2c has a preferential niche interacting with chemosynthetic
462 habitats in relatively low methane fluxes in the Beaufort Sea MVs.
463 The thermal gradients in our study area (see Paull et al., 2015) were substantially higher
464 in the MVs (517.7 mK/m in MV282, 557.9 mK/m in MV420, and 104.3 mK/m in MV740)
465 than in the reference site (28.9 mK/m). In general, high geothermal gradients were observed
466 where methane emission activities were high, as reported at Dvurechenskii MV (Feseker et al.,
467 2009) and Haakon Mosby MV (Kaul et al., 2006). Accordingly, among the MV sites, the
468 methane flux appeared to be the highest at the MV420 site. Indeed, we found a lower abundance
469 of ANME-2c in MV420 than in MV282 and MV740 (Fig. 5, see also Table S2). The MV740
470 site had the lowest thermal gradient of the MV sites, and thus probably the lowest methane flux,

471 which is consistent with the presence of the gas hydrate flake at 230 cm in the MV740 sediment
472 core (see Fig. 1D). At this MV site, ANME-2c occurred at a deeper core depth (0.3–0.7 m) than
473 at the MV282 site (0.0–0.3 m, see also Table S2). This might be linked to the lower methane
474 flux at the MV740 site than at the MV282 site, resulting in penetration of sulfate to deeper
475 sediment depths. Notably, at active MV sites, the sulfate penetration depth can be limited to
476 the upper 2-cm sediment layers (cf. Niemann et al., 2006).
477 Besides ANME-2c, 16S rRNA gene analyses also revealed the presence of ANME-3 (see
478 Table S2). Notably, ANME-3 occurred in MV420 whereas thermal gradients were high
479 (indicating high methane flux) and ANME-2c was almost absent. However, ANME-3 was
480 absent in MV740 where ANME-2c was present. Similar to ANME-2a, ANME-3 was
481 previously found at a high fluid flow/methane flux site associated with *Beggiatoa* mats at the
482 Haakon Mosby Mud Volcano located in Barents Sea at the water depth of 1,250 m (Niemann
483 et al., 2006, Lösekann et al., 2007). Accordingly, it seems that ANME-3 thrives better in a
484 setting with higher methane fluxes than ANME-2c.
485
486 **5 Summary and conclusions**
487 Integrated biogeochemical and nucleic acid analyses were performed for three sediment
488 cores retrieved from active MVs in the Beaufort Sea. The sharp decrease in pore water sulfate
489 concentrations and steep thermal gradients and previous observations of gas flare above the
490 edifices indicate that sulfate-depleted, warm fluids and methane ascend from the Beaufort Sea
491 MVs. We found isotopically depleted lipid biomarkers and nucleic acid signatures of microbial
492 communities, most likely ANME-2c and ANME-3, mediating AOM in the surface sediments
493 at these MVs. The prevalence of ANME-3 over ANME-2c at sites characterized by high
494 thermal gradients (and thus probably high methane fluxes) provides a further indication of a
495 methane-flux driven niche segregation of these ANME-clades. However, the overall

contribution of AOM-related biomass to the organic carbon pool was rather low, and the presence of dominant amounts of lipid biomarkers with comparably high $\delta^{13}C$-values, as well as the dominance of non-ANME sequences, underscores the importance of processes other than AOM in the sediments of the MVs investigated here. Given that our gravity coring system failed to recover the uppermost surface sediments, preventing us from detecting the most active AOM occurrences in the Beaufort Sea MVs, further studies should investigate the undisturbed uppermost surface sediments to investigate the diversity and distribution of AOM-related archaeal communities in detail, and to clarify their preferred habitats in the Beaufort Sea MV systems, for instance, using ROV push cores.

Author contribution

JHK, DHL and YML prepared the manuscript with contributions from AS and HN. DHL, JHK, YML, YKJ, and KHS designed the experiments and were responsible for the analysis. YGK provided thermal gradient data.

Competing interests

The authors declare that they have no conflict of interest.

Acknowledgments

We would like to thank the captain and crew of R/V ARAON for their safe and skillful operation of the ship during the cruise. This study was supported by the KOPRI project (KOPRI-PM18050) funded by the Ministry of Oceans and Fisheries (MOF), and by a National Research Foundation of Korea (NRF) grants funded by the Ministry of Science and ICT (MSIT) (NRF-2016M1A5A1901769, KOPRI-PN18081; NRF-2016R1A2B3015388, KOPRI-PN18100). We also thank Y. Chikaraishi and M. Kaneko for their help in isotope measurements

of biphytanes during a short stay in JAMSTEC, Japan. We are grateful to J.-K. Gal, S. Kang, and D. Kim for their analytical assistance in the laboratory at Hanyang University.

References

Akhmanov, G.G., 1996. Lithology of mud breccia clasts from the Mediterranean Ridge. Marine Geology 132, 151–164.

Akhmanov, G.G., Woodside, J.M., 1998. Mud Volcanic samples in the content of the Mediterranean Ridge Mud Diapiric Belt. In: Robertson, A.H.F., Emeis, K.-C., Richter, C., Camerlenghi, A. (Eds.), Proceed- ings of the ODP, Scientific Results, vol. 160. College Station, Texas, pp. 597–605.

Beal, E. J., House, C. H. and Orphan, V. J.: Manganese- and iron-dependent marine methane oxidation, Science, 325, 184-187, 2009.

Blasco, S., Bennett, R., Brent, T., Burton, M., Campbell, P., Carr, E., Covill, R., Dallimore, S., Davies, E., Hughes-Clarke, J., Issler, D., MacKillop, K., Mazzotti, S., Patton, E., Shearer, J., White, M.: 2010 state of knowledge: Beaufort Sea seabed geohazards associated with offshore hydrocarbon development, Geological Survey of Canada Open File 6989, 340 pp, 2013.

Blumenberg, M., Seifert, R., Reitner, J., Pape, T. and Michaelis, W.: Membrane lipid patterns typify distinct anaerobic methanotrophic consortia, Proc. Natl. Acad. Sci., 101, 11111–11116, 2004.

Boetius, A., Ravenschlag, K., Schubert, C. J., Rickert, D., Widdel, F., Gieseke, A., Amann, R., Jørgensen, B. B., Witte, U. and Pfannkuche, O.: A marine microbial consortium apparently mediating anaerobic oxidation of methane, Nature, 407, 623–626, 2000.

Boetius, A. and Wenzhöfer, F.: Seafloor oxygen consumption fuelled by methane from cold seeps, Nat. Geosci., 6, 725–734, 2013.

546 Bradley, A. S., Hayes, J. M. and Summons, R. E.: Extraordinary ^{13}C enrichment of diether
547 lipids at the Lost City Hydrothermal Field indicates a carbon-limited ecosystem, Geochim.
548 Cosmochim. Acta, 73, 102–118, 2009.
549 Campbell, P., Carr, E., Beaton, F., and Blasco, S. M.: 2009 Beaufort Sea seabed mapping
550 program – operations report, Draft report prepared by Canadian seabed research Ltd. for
551 the geological survey of Canada, 2009.
552 Chevalier, N., Bouloubassi, I., Birgel, D., Cremiere, A., Taphanel, M. H. and Pierre, C.:
553 Authigenic carbonates at cold seeps in the Marmara Sea (Turkey): a lipid biomarker and
554 stable carbon and oxygen isotope investigation, Mar. Geol., 288, 112–121, 2011.
555 Chevalier, N., Bouloubassi, I., Stadnitskaia, A., Taphanel, M. H. and Sinninghe Damsté, J. S.:
556 Lipid biomarkers for anaerobic oxidation of methane and sulphate reduction in cold seep
557 sediments of Nyegga pockmarks (Norwegian margin): Discrepancies in contents and
558 carbon isotope signatures, Geo-Marine Lett., 34, 269–280, 2014.
559 De Rosa, M. and Gambacorta, A.: The Lipids of archaebacteria, Prog. Lipid Res., 27, 153–175,
560 1988.
561 Edgar, R. C., Haas, B. J., Clemente, J. C., Quince, C. and Knight, R.: UCHIME improves
562 sensitivity and speed of chimera detection, Bioinformatics, 27, 2194–2200, 2011.
563 Elvert, M., Suess, E. and Whiticar, M. J.: Anaerobic methane oxidation associated with marine
564 gas hydrates: superlight C-isotopes from saturated and unsaturated C_{20} and C_{25} irregular
565 isoprenoids, Naturwissenschaften, 86, 295–300, 1999.
566 Elvert, M., Hopmans, E. C., Treude, T., Boetius, A. and Suess, E.: Spatial variations of
567 methanotrophic consortia at cold methane seeps: implications from a high-resolution
568 molecular and isotopic approach, Geobiology, 3, 195–209, 2005.
569 Etminan, M., Myhre, G., Highwood, E. J. and Shine, K. P.: Radiative forcing of carbon dioxide,
570 methane, and nitrous oxide: A significant revision of the methane radiative forcing,

571 Geophys. Res. Lett., 43, 12,614–12,623, 2016.
572 Felden, J., Wenzhöfer, F., Feseker, T. and Boetius, A.: Transport and consumption of oxygen
573 and methane in different habitats of the Håkon Mosby Mud Volcano (HMMV), Limnol.
574 Oceanogr., 55, 2366–2380, 2010.
575 Felden, J., Ruff, S. E., Ertefai, T., Inagaki, F. and Hinrichs, K.: Anaerobic methanotrophic
576 community of a 5346-m-deep vesicomyid clam colony in the Japan Trench, Geobiology,
577 12, 2014.
578 Felsenstein, J.: Evolutionary Trees from DNA Sequences : A Maximum Likelihood Approach,
579 J. Mol. Evol., 17, 368–376, 1981.
580 Ferrante, G., Ekiel, I., Patel, G. B. and Sprott, G. D.: A novel core lipid isolated from the
581 aceticlastic methanogen, *Methanothrix concilii* GP6, Biochim. Biophys. Acta - Lipids
582 Lipid Metab., 963, 173–182, 1988.
583 Feseker, T., Pape, T., Wallmann, K., Klapp, S. A., Schmidt-Schierhorn, F. and Bohrmann, G.:
584 The thermal structure of the Dvurechenskii mud volcano and its implications for gas
585 hydrate stability and eruption dynamics, Mar. Pet. Geol., 26, 1812–1823, 2009.
586 Haese, R. R., Meile, C., Van Cappellen, P. and De Lange, G. J.: Carbon geochemistry of cold
587 seeps: Methane fluxes and transformation in sediments from Kazan mud volcano, eastern
588 Mediterranean Sea, Earth Planet. Sci. Lett., 212, 361–375, 2003.
589 Haroon, M. F., Hu, S., Shi, Y., Imelfort, M., Keller, J., Hugenholtz, P., Yuan, Z. and Tyson, G.
590 W.: Anaerobic oxidation of methane coupled to nitrate reduction in a novel archaeal
591 lineage, Nature, 500, 567-570, 2013.
592 Himmler, T., Birgel, D., Bayon, G., Pape, T., Ge, L., Bohrmann, G. and Peckmann, J.:
593 Formation of seep carbonates along the Makran convergent margin , northern Arabian Sea
594 and a molecular and isotopic approach to constrain the carbon isotopic composition of
595 parent methane, Chem. Geol., 415, 102–117, 2015.

596 Hinrichs, K. U. and Boetius, A.: The anaerobic oxidation of methane: new insights in microbial
597 ecology and biogeochemistry, edited by G. Wefer, D. Billett, D. Hebbeln, B. B. Jørgensen,
598 M. Schlüter, and T. Van Weering, Springer-Verlag, Berlin, Germany, 2002.
599 Hwang, K., Oh, J., Kim, T. K., Kim, B. K., Yu, D. S., Hou, B. K., Caetano-Anollés, G., Hong,
600 S. G. and Kim, K. M.: CLUSTOM: a novel method for clustering 16S rRNA next
601 generation sequences by overlap minimization, PLoS One, 8, e62623, 2013.
602 Huguet, C., Hopmans, E. C., Febo-Ayala, W., Thompson, D. H., Sinninghe Damsté, J. S. and
603 Schouten, S.: An improved method to determine the absolute abundance of glycerol
604 dibiphytanyl glycerol tetraether lipids, Org. Geochem., 37, 1036–1041, 2006.
605 Inagaki, F., Nunoura, T., Nakagawa, S., Teske, A., Lever, M., Lauer, A., Suzuki, M., Takai, K.,
606 Delwiche, M., Colwell, F. S., Nealson, K. H., Horikoshi, K., D'Hondt, S. and Jorgensen,
607 B. B.: Biogeographical distribution and diversity of microbes in methane hydrate-bearing
608 deep marine sediments on the Pacific Ocean Margin, Proc. Natl. Acad. Sci., 103, 2815–
609 2820, 2006.
610 Ivanov, M.K., Limonov, A.F., Woodside, J.M., 1992. Geological and geophysical
611 investigations in the Mediterranean and Black Seas. Initial results of the ''Training-
612 through-Research'' Cruise of R/V Gelendzhik in the Eastern Mediterranean and the Black
613 Sea (June/July 1991), UNESCO Reports in Marine Sciences, 56.
614 Ivanov, M.K., Limonov, A.F., Woodside, J.M., 1998. Extensive deep fluid flux through the sea
615 floor on the Crimean continental margin (Black Sea). In: Henriet, J.-P., Mienert, J. (Eds.),
616 Gas Hydrates. Relevance to World Margin Stability and Climatic Change. Geological
617 Society, London, pp. 195–213 Special Publications, 137.
618 James, R. H., Bousquet, P., Bussmann, I., Haeckel, M., Kipfer, R., Leifer, I., Niemann, H.,
619 Ostrovsky, I., Piskozub, J., Rehder, G., Treude, T., Vielstädte, L., Greinert, J.: Effects of
620 climate change on methane emissions from seafloor sediments in the Arctic Ocean: A

review, Limnol. Oceanogr., 61, 283–299, 2016.

Jiang, L., Zheng, Y., Chen, J., Xiao, X. and Wang, F.: Stratification of archaeal communities in shallow sediments of the Pearl River Estuary, Southern China, Antonie van Leeuwenhoek, Int. J. Gen. Mol. Microbiol., 99, 739–751, 2011.

Kaneko, M., Kitajima, F. and Naraoka, H.: Stable hydrogen isotope measurement of archaeal ether-bound hydrocarbons, Org. Geochem., 42, 166–172, 2011.

Kaneko, M., Naraoka, H., Takano, Y. and Ohkouchi, N.: Distribution and isotopic signatures of archaeal lipid biomarkers associated with gas hydrate occurrences on the northern Cascadia Margin, Chem. Geol., 343, 76–84, 2013.

Kaul, N., Foucher, J. P. and Heesemann, M.: Estimating mud expulsion rates from temperature measurements on Håkon Mosby Mud Volcano, SW Barents Sea, Mar. Geol., 229, 1–14, 2006.

Kim, J., Lee, D., Yoon, S., Jeong, K., Choi, B. and Shin, K.: Chemosphere Contribution of petroleum-derived organic carbon to sedimentary organic carbon pool in the eastern Yellow Sea (the northwestern Pacific), Chemosphere, 168, 1389–1399, 2017.

Kim, O. S., Cho, Y. J., Lee, K., Yoon, S. H., Kim, M., Na, H., Park, S. C., Jeon, Y. S., Lee, J. H., Yi, H., Won, S. and Chun, J.: Introducing EzTaxon-e: A prokaryotic 16s rRNA gene sequence database with phylotypes that represent uncultured species, Int. J. Syst. Evol. Microbiol., 62, 716–721, 2012.

Knittel, K., Lösekann, T., Boetius, A., Kort, R., Amann, R. and Lo, T.: Diversity and Distribution of Methanotrophic Archaea at Cold Seeps Diversity and Distribution of Methanotrophic Archaea at Cold Seeps, Appl. Environ. Microbiol., 71, 467–479, 2005.

Knittel, K. and Boetius, A.: Anaerobic oxidation of methane: Progress with an unknown process, Annu. Rev. Microbiol., 63, 311–334, 2009.

Koga, Y., Nishihara, M., Morii, H. and Akagawa-Matsushita, M.: Ether polar lipids of

methanogenic bacteria: Structures, comparative aspects, and biosyntheses, Microbiol. Rev., 57, 164–182, 1993.

Koga, Y., Morii, H., Akagawa-Matsushita, M. and Ohga, M.: Correlation of Polar Lipid Composition with 16S rRNA Phylogeny in Methanogens. Further Analysis of Lipid Component Parts, Biosci. Biotechnol. Biochem., 62, 230–236, 1998.

Koga, Y. and Morii, H.: Recent Advances in Structural Research on Ether Lipids from Archaea Including Comparative and Physiological Aspects, Biosci. Biotechnol. Biochem., 69, 2019–2034, 2005.

Kopf, A. J.: Significance of mud volcanism, Rev. Geophys., 40, 2–46, 2002.

Kushwaha, S. C. and Kates, M.: 2, 3-Di-O-phytanyl-sn-glycerol and prenols from extremely halophilic bacteria, Phytochemistry, 17, 2029–2030, 1978.

Lee, D. H., Kim, J. H., Bahk, J. J., Cho, H. Y., Hyun, J. H. and Shin, K. H.: Geochemical signature related to lipid biomarkers of ANMEs in gas hydrate-bearing sediments in the Ulleung Basin, East Sea (Korea), Mar. Pet. Geol., 47, 125–135, 2013.

Levitus, S., Antonov, J. I., Boyer, T. P. and Stephens, C.: Warming of the world ocean, Science., 287, 2225–2229, 2000.

Li, Q., Wang, F., Chen, Z., Yin, X. and Xiao, X.: Stratified active archaeal communities in the sediments of Jiulong River estuary, China, Front. Microbiol., 3, 1–14, 2012.

Liu, X., Lipp, J. S. and Hinrichs, K.-U.: Distribution of intact and core GDGTs in marine sediments, Org. Geochem., 42, 368–375, 2011.

Lösekann, T., Knittel, K., Nadalig, T., Fuchs, B., Niemann, H., Boetius, A. and Amann, R.: Diversity and Abundance of Aerobic and Anaerobic Methane Oxidizers at the Haakon Mosby Mud Volcano, Barents Sea, Appl. Environ. Microbiol., 73, 3348–3362, 2007.

Marín-Moreno, H., Giustiniani, M., Tinivella, U. and Piñero, E.: The challenges of quantifying the carbon stored in Arctic marine gas hydrate, Mar. Pet. Geol., 71, 76–82, 2016.

671 Milkov, A. V., Sassen, R., Apanasovich, T. V. and Dadashev, F. G.: Global gas flux from mud
672 volcanoes: A significant source of fossil methane in the atmosphere and the ocean,
673 Geophys. Res. Lett., 30, 17–20, 2003.
674 Mulicka, J., Ferdelman, T. G., Polerecky, L., Franzke, D., Wegner, G., Schmid, M., Lieberwirth,
675 I., Wagner, M., Widdel, F., Kuyper, M. M. M.: Zero-valent sulphur is a key intermediate
676 in marine methane oxidation, Nature, 491, 541–546, 2012.
677 Nauhaus, K., Albrecht, M., Elvert, M., Boetius, A. and Widdel, F.: In vitro cell growth of marine
678 archaeal-bacterial consortia during anaerobic oxidation of methane with sulfate, Environ.
679 Microbiol., 9, 187–196, 2007.
680 Niemann, H., Elvert, M., Hovland, M., Orcutt, B., Judd, A., Suck, I., Gutt, J., Damm, E., Finster,
681 K. and Boetius, A.: Methane emission and consumption at a North Sea gas seep
682 (Tommeliten area), Biogeosciences, 2, 1197–1241, 2005.
683 Niemann, H., Lösekann, T., de Beer, D., Elvert, M., Nadalig, T., Knittel, K., Amann, R., Sauter,
684 E. J., Schlüter, M., Klages, M., Foucher, J. P. and Boetius, A.: Novel microbial
685 communities of the Haakon Mosby mud volcano and their role as a methane sink, Nature,
686 443, 854–858, 2006.
687 Niemann, H. and Elvert, M.: Diagnostic lipid biomarker and stable carbon isotope signatures
688 of microbial communities mediating the anaerobic oxidation of methane with sulphate,
689 Org. Geochem., 39, 1668–1677, 2008.
690 Oh, J., Kim, B. K., Cho, W. S., Hong, S. G. and Kim, K. M.: PyroTrimmer: A software with
691 GUI for pre-processing 454 amplicon sequences, J. Microbiol., 50, 766–769, 2012.
692 Orphan, V. J., Hinrichs, K., Iii, W. U., Paull, C. K., Taylor, L. T., Sylva, S. P., Hayes, J. M. and
693 Delong, E. F.: Comparative Analysis of Methane-Oxidizing Archaea and Sulfate-Reducing
694 Bacteria in Anoxic Marine Sediments, Appl. Environ. Microbiol., 67, 1922–1934, 2001.
695 Pancost, R. D., Sinninghe Damsté, J. S., Lint, S. D., van der Maarel, M. J. E. C., Gottschal, J.

696 C. and Shipboard Scientific Party: Biomarker evidence for widespread anaerobic methane
697 oxidation in Mediterranean sediments by a consortium of methanogenic archaea and
698 bacteria, Appl Environ. Microbiol., 66, 1126–1132, 2000.
699 Pancost, R. D., Bouloubassi, I., Aloisi, G. and Sinninghe Damsté, J. S.: Three series of non-
700 isoprenoidal dialkyl glycerol diethers in cold-seep carbonate crusts, Org. Geochem., 32,
701 695–707, 2001a.
702 Pancost, R. D., Hopmans, E. C., Sinninghe Damsté, J. S. and Scientific Party, the M. S.:
703 Archaeal lipids in mediterranean cold seeps: Molecular proxies for anaerobic methane
704 oxidation, Geochim. Cosmochim. Acta, 65, 1611–1627, 2001b.
705 Pancost, R. D., McClymont, E. L., Bingham, E. M., Roberts, Z., Charman, D. J., Hornibrook,
706 E. R. C., Blundell, A., Chambers, F. M., Lim, K. L. H. and Evershed, R. P.: Archaeol as a
707 methanogen biomarker in ombrotrophic bogs, Org. Geochem., 42, 1279–1287, 2011.
708 Paull, C. K., Ussler, W., Dallimore, S. R., Blasco, S. M., Lorenson, T. D., Melling, H., Medioli,
709 B. E., Nixon, F. M. and McLaughlin, F. A.: Origin of pingo-like features on the Beaufort
710 Sea shelf and their possible relationship to decomposing methane gas hydrates, Geophys.
711 Res. Lett., 34, 1–5, 2007.
712 Paull, C. K., Dallimore, S., Hughes, J., Blasco, S., Lundsten, E., Ussler III, W., Graves, D.,
713 Sherman, A., Conway, K., Melling, H., Vagle, S. and Collett, T.: Tracking the
714 decomposition of submarine permafrost and gas hydrate under the shelf and slope of the
715 Beaufort Sea, in in Proceedings of the 7th International Conference on Gas Hydrates, vol.
716 1, pp. 1689–1699., 2011.
717 Paull, C. K., Dallimore, S. R., Caress, D. W., Gwiazda, R., Melling, H., Riedel, M., Jin, Y. K.,
718 Hong, J. K., Kim, Y.-G., Graves, D., Sherman, A., Lundsten, E., Anderson, K., Lundsten,
719 L., Villinger, H., Kopf, A., Johnson, S. B., Clarke, J. H., Blas, S., Conway, K., Neelands,
720 P., Thomas, H. and Cote, M.: Active mud volcanoes on the continental slope of the

721 Canadian Beaufort Sea, Geochem. Geophys. Geosyst., 16, 1541–1576, 2015.
722 Polyakov, I. V., Timokhov, L. A., Alexeev, V. A., Bacon, S., Dmitrenko, I. A., Fortier, L., Frolov,
723 I. E., Gascard, J.-C., Hansen, E., Ivanov, V. V., Laxon, S., Mauritzen, C., Perovich, D.,
724 Shimada, K., Simmons, H. L., Sokolov, V. T., Steele, M. and Toole, J.: Arctic Ocean
725 Warming Contributes to Reduced Polar Ice Cap, J. Phys. Oceanogr., 40, 2010.
726 Reeburgh, W. S.: Oceanic Methane Biogeochemistry, Chem. Rev., 107, 486–513, 2007.
727 Roalkvam, I., Jørgensen, S. L., Chen, Y., Stokke, R., Dahle, H., Hocking, W. P., Lanzén, A.,
728 Haflidason, H. and Steen, I. H.: New insight into stratification of anaerobic methanotrophs
729 in cold seep sediments, FEMS Microbiol. Ecol., 78, 233–243, 2011.
730 Rossel, P. E., Elvert, M., Ramette, A., Boetius, A. and Hinrichs, K. U.: Factors controlling the
731 distribution of anaerobic methanotrophic communities in marine environments: Evidence
732 from intact polar membrane lipids, Geochim. Cosmochim. Acta, 75, 164–184, 2011.
733 Sahling, H., Rickert, D., Lee, R. W., Linke, P. and Suess, E.: Macrofaunal community structure
734 and sulfide flux at gas hydrate deposits from the Cascadia convergent margin, NE Pacific,
735 Mar. Ecol. Prog. Ser., 231, 121–138, 2002.
736 Saint-ange, F., Kuus, P., Blasco, S., Piper, D. J. W., Hughes, J. and Mackillop, K.: Multiple
737 failure styles related to shallow gas and fluid venting, upper slope Canadian Beaufort Sea,
738 northern Canada, Mar. Geol., 355, 136–149, 2014.
739 Schouten, S., Huguet, C., Hopmans, E. C., Kienhuis, M. V. M. and Sinninghe Damsté, J. S.:
740 Analytical methodology for TEX_{86} paleothermometry by high-performance liquid
741 chromatography/atmospheric pressure chemical ionization-mass spectrometry, Anal.
742 Chem., 79, 2940–2944, 2007.
743 Schouten, S., Hopmans, E. C. and Sinninghe Damsté, J. S.: The organic geochemistry of
744 glycerol dialkyl glycerol tetraether lipids : a review, Org. Geochem., 54, 19–61, 2013.
745 Shnukov, E.F., Starostenko, V.I., Rusakov, O.M., Kobolev, V.P., Maslakov, N.A., 2005. Gas

volcanism in the Black Sea. Abstract. International Workshop on Methane in Sediments and Water Column of the Black Sea: Formation, Transport, Pathways and the Role Within the Carbon Cycle. Sevastopol, Ukraine, pp. 50–51.

Sprott, G. D., Dicaire, C. J., Choquet, C. G., Patel, G. B., Ekiel, I. and Dennis, G.: Hydroxydiether Lipid Structures in Hydroxydiether Lipid Structures in Methanosarcina Methanococcus voltaet, Appl. Environ. Microbiol., 59, 912–914, 1993.

Stadnitskaia, A., Ivanov, M. K. and Damsté, J. S. S.: Application of lipid biomarkers to detect sources of organic matter in mud volcano deposits and post-eruptional methanotrophic processes in the Gulf of Cadiz , NE Atlantic, Mar. Geol., 255, 1–14, 2008a.

Stadnitskaia, A., Nadezhkin, D., Abbas, B., Blinova, V., Ivanov, M. K. and Damste, J. S. S.: Carbonate formation by anaerobic oxidation of methane: Evidence from lipid biomarker and fossil 16S rDNA, Geochim. Cosmochim. Acta, 72, 1824–1836, 2008b.

Tamura, K., Stecher, G., Peterson, D., Filipski, A. and Kumar, S.: MEGA6: Molecular evolutionary genetics analysis version 6.0, Mol. Biol. Evol., 30, 2725–2729, 2013.

Tryon, M. D., Brown, K. M., Torres, M. E., Tréhu, A. M., McManus, J. and Collier, R. W.: Measurements of transience and downward fluid flow near episodic methane gas vents, Hydrate Ridge, Cascadia, Geology, 27, 1075–1078, 1999.

Weijers, J. W. H., Lim, K. L. H., Aquilina, A., Sinninghe Damsté, J. S. and Pancost, R. D.: Biogeochemical controls on glycerol dialkyl glycerol tetraether lipid distributions in sediments characterized by diffusive methane flux, Geochem. Geophys. Geosyst., 12, Q10010, 2011.

Werne, J., Baas, B. and Damsté, J. S. S.: Molecular isotopic tracing of carbon flow and trophic relationships in a methane supported microbial community, Limnol. Oceanogr., 47, 1694–1701, 2002.

Werne, J. P., Haese, R. R., Zitter, T., Aloisi, G., Bouloubassi, I., Heijs, S., Fiala-Médioni, A.,

771 Pancost, R. D., Sinninghe Damsté, J. S., de Lange, G., Forney, L. J., Gottschal, J. C.,
772 Foucher, J. P., Mascle, J. and Woodside, J.: Life at cold seeps: A synthesis of
773 biogeochemical and ecological data from Kazan mud volcano, eastern Mediterranean Sea,
774 Chem. Geol., 205, 367–390, 2004.
775 Westbrook, G. K., Thatcher, K. E., Rohling, E. J., Piotrowski, A. M., Pälike, H., Osborne, A.
776 H., Nisbet, E. G., Minshull, T. A., Lanoisellé, M., James, R. H., Hühnerbach, V., Green,
777 D., Fisher, R. E., Crocker, A. J., Chabert, A., Bolton, C., Beszczynska-Möller, A., Berndt,
778 C. and Aquilina, A.: Escape of methane gas from the seabed along the West Spitsbergen
779 continental margin, Geophys. Res. Lett., 36, 2009.
780 Whiticar, M. J.: Carbon and hydrogen isotope systematics of bacterial formation and oxidation
781 of methane, Chem. Geol., 161, 291–314, 1999.
782 Wuebbles, D. J. and Hayhoe, K.: Atmospheric methane and global change, Earth-Sci. Rev., 57,
783 177–210, 2002.
784 Zhang, C. L., Pancost, R. D., Sassen, R., Qian, Y. and Macko, S. A.: Archaeal lipid biomarkers
785 and isotopic evidence of anaerobic methane oxidation associated with gas hydrates in the
786 Gulf of Mexico, Org. Geochem., 34, 827–836, 2003.
787 Zhang, Y. G., Zhang, C. L., Liu, X.-L., Li, L., Hinrichs, K.-U. and Noakes, J. E.: Methane Index:
788 A tetraether archaeal lipid biomarker indicator for detecting the instability of marine gas
789 hydrates, Earth Planet. Sci. Lett., 307, 525–534, 2011.
790

791 **Table Legends**

792 Table 1. Results of total organic carbon (TOC) contents, $\delta^{13}C$ of TOC, and concentrations and
793 stable carbon isotopes of selected lipid biomarkers such as isoprenoid DGDs, non-isoprenoid
794 DGDs, and biphytanes derived from isoprenoid GDGTs.

795

796

797 **Figure captions**

798

799 Fig. 1. (A) Map showing the study area (red box) with inset regional map of Alaska and
800 northwestern Canada modified from Paull et al. (2015). (B) Map showing the three mud
801 volcano (MV) locations on the upper slope of the Beaufort Sea. (C) Detailed bathymetric maps
802 showing the locations of sediment cores ARA05C-10-GC (MV282), ARA05C-01-GC
803 (MV420), and ARA05C-18-GC (MV740). (D) Lithology of the three sediment cores
804 investigated.

805

806 Fig. 2. Depth profiles of sulphate (SO_4^{2-}) concentrations, total organic carbon (TOC) content,
807 and $\delta^{13}C_{TOC}$ in sediment cores from MV282, MV420, and MV740. Grey hatched bars indicate
808 gas-gaps in the sediment layers. Note that the sulphate concentration data are from Paull et al.
809 (2015).

810

811 Fig. 3. Vertical profiles of selected lipid biomarkers (archaeol, hydroxyarchaeol, and DGD (If))
812 obtained from sediment cores (A) ARA05C-10-GC (MV282), (B) ARA05C-01-GC (MV420),
813 and (C) ARA05C-18-GC (MV740). Grey hatched bars indicate gas gaps in sediment layers.

814

Fig. 4. HPLC/APCI-MS base peak chromatograms of polar fractions obtained from sediment cores (A) ARA05C-10-GC (MV282), (B) ARA05C-01-GC (MV420), and (C) ARA05C-18-GC (MV740). Note that the Roman numerals (I, II, III, IV and V) refer to GDGT-0, GDGT-1, GDGT-2, GDGT-3, and crenarchaeol, respectively. The Arabic numbers in GDGT-0, GDGT-1, GDGT-2, and GDGT-3 indicate the number of cyclopentane rings within the biphytane chains.

Fig. 5. Phylogenetic tree based on 16S rRNA showing the relationships of methanomicrobial sequences recovered in this study with selected reference sequences of the domain Euryarchaeota. The phylogenetic tree was inferred by the maximum-likelihood method. Bootstrap values of >70 are shown on corresponding branches. The scale bar indicates evolutionary distance of 0.05 substitutions per site.

827 Table 1

Core depth	TOC	$\delta^{13}C_{TOC}$	Lipid biomarkers																	hydroxyarchaeol/archaeol
			Archaeol		*sn*-2-hydroxyarchaeol		*sn*-3-hydroxyarchaeol		Non-isoprenoid DGDs		GDGT-0	GDGT-1	GDGT-2	GDGT-3	Crenarchaeol	Biphytane 0	Biphytane 1	Biphytane 2	Biphytane 3	
(mbsf)	(wt. %)	(‰ VPDB)	µg/g dw	‰ VPDB	µg/g dw	‰ VPDB	µg/g dw	‰ VPDB	µg/g dw	‰ VPDB	µg/g dw	µg/g dw	µg/g dw	µg/g dw	µg/g dw	‰ VPDB	‰ VPDB	‰ VPDB	‰ VPDB	
MV282																				
0.02	1.2	-26.6	0.05	-65.0	0.09	-107.4	0.02	n.d.	0.13	-39.4	0.07	0.01	0.01	0.00	0.09	-29.4	-46.2	-39.0	-27.1	1.8
0.09	1.5	-26.6	0.09	-67.7	0.13	-100.6	0.03	n.d.	0.15	-40.1	0.07	0.01	0.01	0.01	0.08	-32.3	-63.4	-30.9	-26.8	1.6
0.20	1.1	-26.4	0.06	-62.0	0.11	-103.2	0.03	-92.8	0.16	-41.4	0.06	0.01	0.01	0.00	0.06	-33.9	-46.3	-28.6	-26.6	1.7
0.33	1.2	-26.4	0.07	-60.3	0.09	-98.6	0.02	n.d.	0.16	-37.9	0.05	0.01	0.01	0.00	0.05	-	-	-	-	1.3
0.50	1.3	-26.2	0.06	-64.8	0.07	-99.4	0.02	-84.2	0.13	-45.3	0.05	0.01	0.00	0.00	0.05	-36.4	n.d.	-21.2	-29.6	1.3
0.88	1.5	-26.0	0.06	-60.9	0.07	-103.6	0.02	n.d.	0.12	-42.9	0.05	0.01	0.01	0.00	0.05	-	-	-	-	1.3
1.05	1.4	-26.2	0.06	-60.8	0.08	-91.0	0.02	-87.3	0.14	-36.0	0.05	0.01	0.01	0.00	0.06	-32.2	-36.0	-29.0	-16.7	1.5
1.30	1.4	-26.2	0.06	-63.7	0.08	-97.3	0.02	n.d.	0.14	-39.3	0.06	0.01	0.01	0.01	0.06	-	-	-	-	1.3
1.60	1.5	-26.0	0.06	-61.8	0.08	-98.1	0.02	-89.1	0.14	-38.8	0.05	0.01	0.00	0.00	0.05	-33.5	-38.6	-30.7	-37.6	1.5
1.90	1.2	-26.5	0.03	-59.2	0.03	-96.0	0.01	n.d.	0.06	-43.8	0.02	0.00	0.00	0.00	0.02	-	-	-	-	1.3
MV420																				
0.08	1.0	-26.4	0.03	-58.6	0.02	-113.8	n.d.	n.d.	0.09	-34.3	0.12	0.01	0.01	0.01	0.07	-42.7	n.d.	n.d.	n.d.	0.5
0.20	1.1	-26.3	0.04	-41.7	0.01	-86.8	n.d.	n.d.	0.11	-36.6	0.19	0.02	0.01	0.01	0.12	-	-	-	-	0.2
0.33	1.1	-26.2	0.04	-47.6	0.02	-108.8	n.d.	n.d.	0.15	-31.9	0.06	0.00	0.00	0.00	0.05	-34.0	-61.6	-22.9	-24.0	0.6
0.50	1.1	-26.1	0.03	-38.6	0.00	-94.6	n.d.	n.d.	0.11	-34.3	0.03	0.00	0.00	0.00	0.02	-	-	-	-	0.1
0.70	1.1	-26.7	0.09	-79.8	0.13	-113.9	0.08	-93.1	0.25	-46.9	0.10	0.01	0.01	0.01	0.13	-30.3	-51.4	-28.4	-24.0	1.4
0. 88	1.2	-26.2	0.06	-49.0	0.03	-94.7	n.d.	n.d.	0.10	-41.0	0.06	0.01	0.01	0.01	0.04	-	-	-	-	0.5
1.05	1.2	-26.0	0.06	-44.2	0.03	-92.4	0.02	n.d.	0.09	-40.2	0.07	0.01	0.01	0.01	0.06	-32.3	-55.7	-30.1	-30.4	0.5
1.38	1.1	-26.1	0.06	-45.6	0.02	-95.7	n.d.	n.d.	0.11	-41.5	0.07	0.01	0.01	0.01	0.06	-	-	-	-	0.3
1.6	1.2	-26.1	0.08	-45.3	0.03	-97.0	n.d.	n.d.	0.11	-37.2	0.08	0.01	0.01	0.01	0.07	-34.8	-46.8	-29.4	-28.2	0.4
1.81	1.2	-26.0	0.07	-47.7	0.03	-86.4	n.d.	n.d.	0.09	-40.1	0.30	0.04	0.05	0.03	0.25	-	-	-	-	0.4
2.17	1.3	-26.1	0.06	-44.8	0.02	-92.1	n.d.	n.d.	0.09	-39.9	0.27	0.03	0.04	0.03	0.22	-	-	-	-	0.4
MV740																				
0.08	1.2	-26.3	0.04	-38.5	0.02	-86.2	n.d.	n.d.	0.11	-34.3	0.07	0.01	0.01	0.01	0.05	-36.2	-49.5	-26.8	-25.3	0.5
0.20	1.1	-26.3	0.04	-43.6	0.02	-87.8	n.d.	n.d.	0.11	-32.6	0.07	0.01	0.01	0.01	0.05	-	-	-	-	0.5
0.35	1.3	-26.4	0.05	-59.6	0.05	-102.4	n.d.	n.d.	0.12	-37.9	0.09	0.01	0.01	0.01	0.07	-36.1	-57.0	-24.6	-31.7	0.9
0. 45	1.1	-26.4	0.04	-69.6	0.05	-103.7	n.d.	n.d.	0.12	-37.5	0.09	0.01	0.01	0.01	0.06	-31.5	-56.0	-25.2	-31.4	1.1
0.55	1.2	-26.5	0.05	-65.1	0.05	-103.3	n.d.	n.d.	0.10	-42.7	0.06	0.01	0.01	0.01	0.05	-40.5	-50.6	-27.2	-30.7	1.0
0. 75	1.1	-26.2	0.04	-58.3	0.02	-93.5	n.d.	n.d.	0.11	-40.4	0.08	0.01	0.01	0.01	0.05	-	-	-	-	0.7
1.00	1.2	-26.1	0.04	-59.5	0.01	-93.7	n.d.	n.d.	0.09	-36.7	0.09	0.01	0.01	0.01	0.07	-31.0	-55.5	-31.4	-26.8	0.3
1.13	1.1	-26.2	0.03	-54.4	0.01	-96.7	n.d.	n.d.	0.09	-37.4	0.08	0.01	0.01	0.01	0.05	-	-	-	-	0.5
1.55	1.3	-26.4	0.03	-53.9	0.01	-93.0	n.d.	n.d.	0.08	-33.8	0.07	0.01	0.01	0.01	0.06	-33.4	-50.5	-27.0	-23.5	0.4
2.00	1.2	-26.2	0.04	-41.2	0.01	-82.1	n.d.	n.d.	0.09	-35.7	0.09	0.01	0.01	0.01	0.06	-	-	-	-	0.3
2.30	1.2	-26.3	0.04	-52.8	0.02	-88.8	n.d.	n.d.	0.09	-38.6	0.08	0.01	0.01	0.01	0.06	-34.1	n.d.	n.d.	n.d.	0.4
2.60	1.1	-26.4	0.03	-55.0	0.02	-90.1	n.d.	n.d.	0.08	-37.3	0.06	0.01	0.01	0.01	0.05	-	-	-	-	0.5

828

829

830

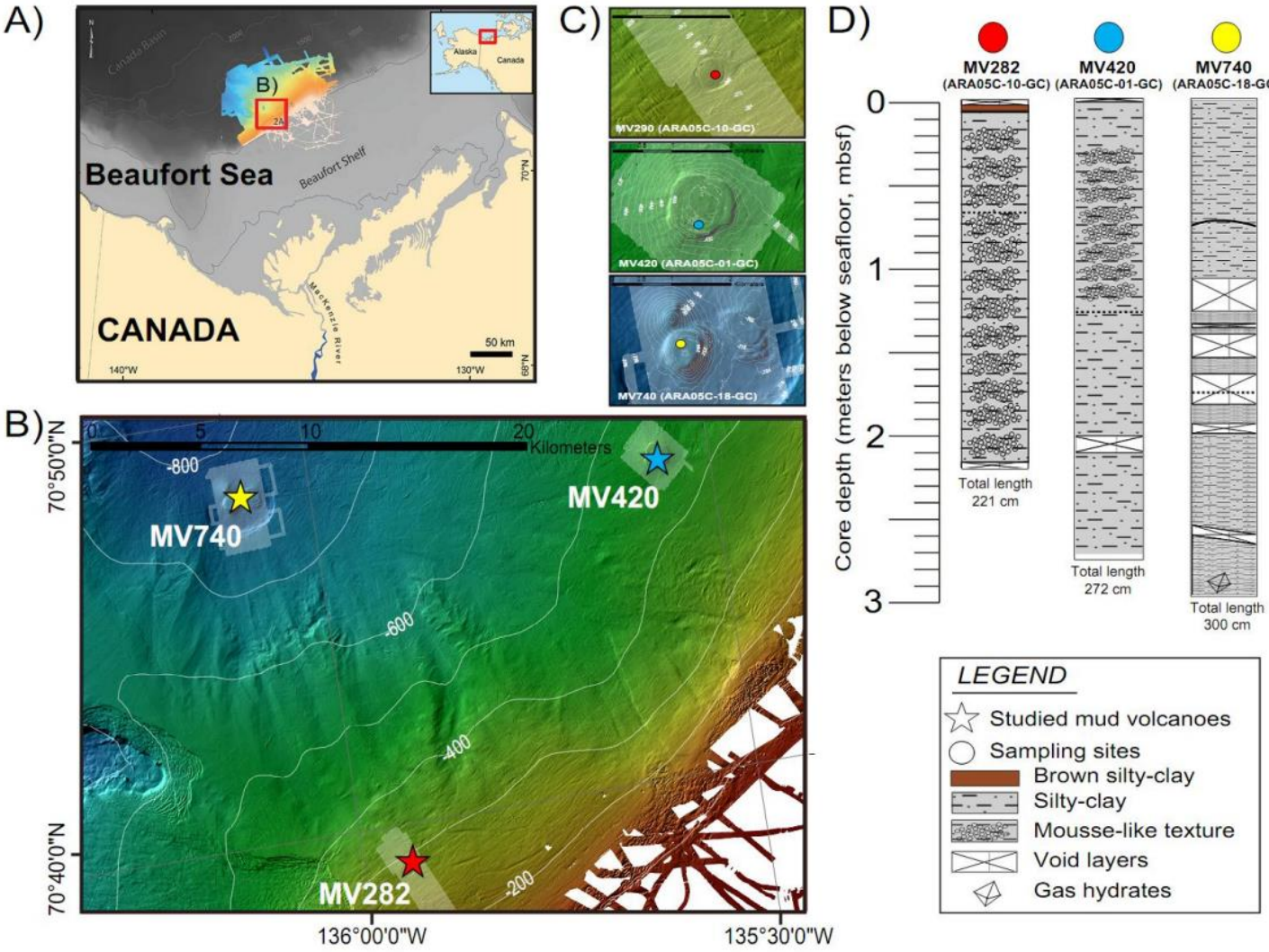
A)
Beaufort Sea
Beaufort Shelf
CANADA
Alaska
Canada
50 km
140°W
130°W
70°N
B)
C)
MV290 (ARA05C-10-GC)
MV420 (ARA05C-01-GC)
MV740 (ARA05C-18-GC)
D)
MV282
(ARA05C-10-GC)
MV420
(ARA05C-01-GC)
MV740
(ARA05C-18-GC)
Core depth (meters below seafloor, mbsf)
0
1
2
3
Total length
221 cm
Total length
272 cm
Total length
300 cm
B)
0
5
10
20
Kilometers
-800
-600
-400
-200
MV740
MV420
MV282
70°50'0"N
70°40'0"N
136°00'0"W
135°30'0"W
LEGEND
Studied mud volcanoes
Sampling sites
Brown silty-clay
Silty-clay
Mousse-like texture
Void layers
Gas hydrates

Fig. 1

831

832

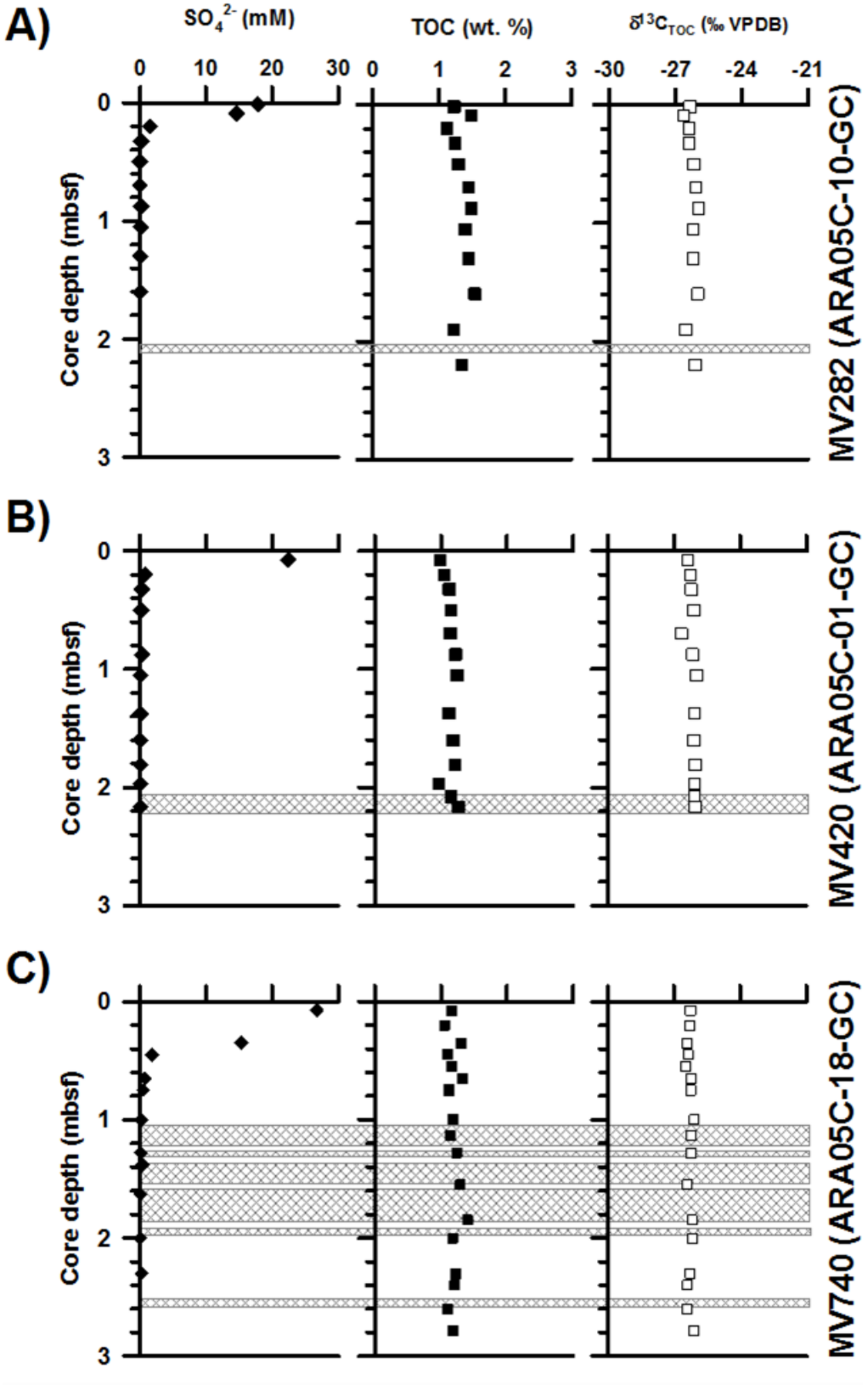
A)
SO_4^{2-} (mM)
TOC (wt. %)
$\delta^{13}C_{TOC}$ (‰ VPDB)
0 10 20 30
0 1 2 3
-30 -27 -24 -21
Core depth (mbsf)
0 1 2 3
MV282 (ARA05C-10-GC)
B)
Core depth (mbsf)
0 1 2 3
MV420 (ARA05C-01-GC)
C)
Core depth (mbsf)
0 1 2 3
MV740 (ARA05C-18-GC)

Fig. 2

833

834

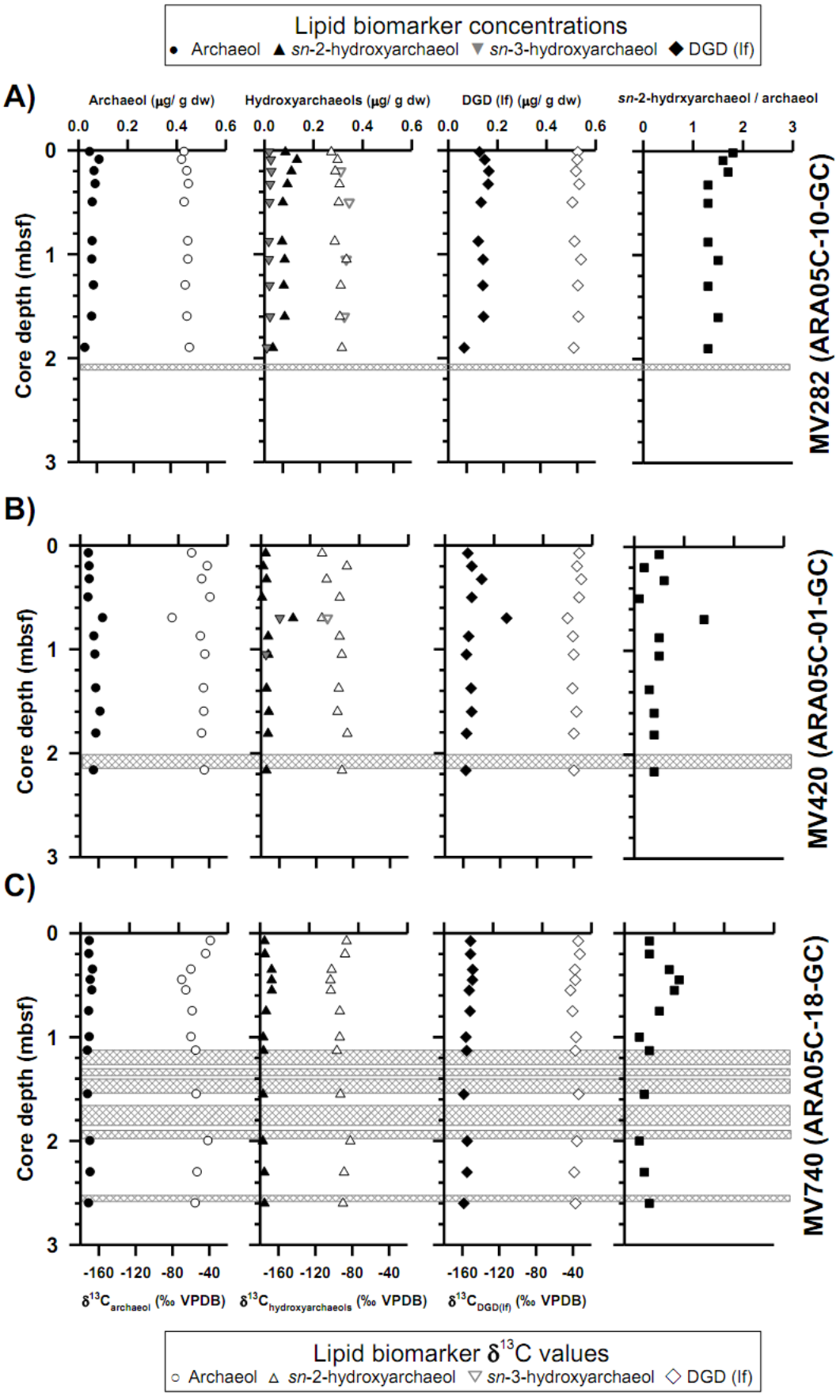
Lipid biomarker concentrations
Archaeol
sn-2-hydroxyarchaeol
sn-3-hydroxyarchaeol
DGD (lf)
A)
B)
C)
Archaeol (µg/ g dw)
Hydroxyarchaeols (µg/ g dw)
DGD (lf) (µg/ g dw)
sn-2-hydrxyarchaeol / archaeol
Core depth (mbsf)
MV282 (ARA05C-10-GC)
MV420 (ARA05C-01-GC)
MV740 (ARA05C-18-GC)
δ13Carchaeol (‰ VPDB)
δ13Chydroxyarchaeols (‰ VPDB)
δ13CDGD(lf) (‰ VPDB)
Lipid biomarker δ13C values
Archaeol
sn-2-hydroxyarchaeol
sn-3-hydroxyarchaeol
DGD (lf)

Fig. 3

835

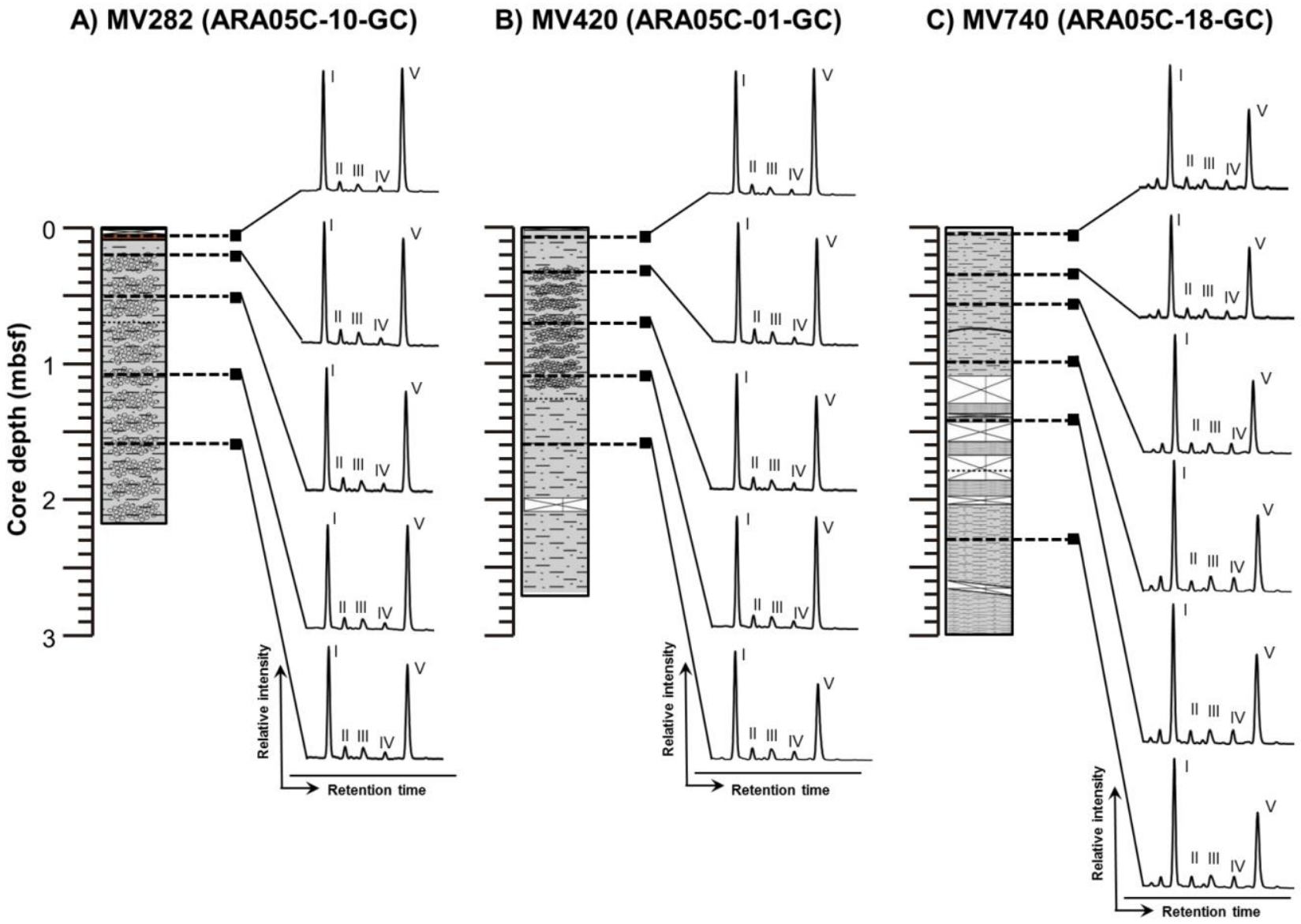
A) MV282 (ARA05C-10-GC)
B) MV420 (ARA05C-01-GC)
C) MV740 (ARA05C-18-GC)
Core depth (mbsf)
0
1
2
3
I
II
III
IV
V
Relative intensity
Retention time

Fig. 4

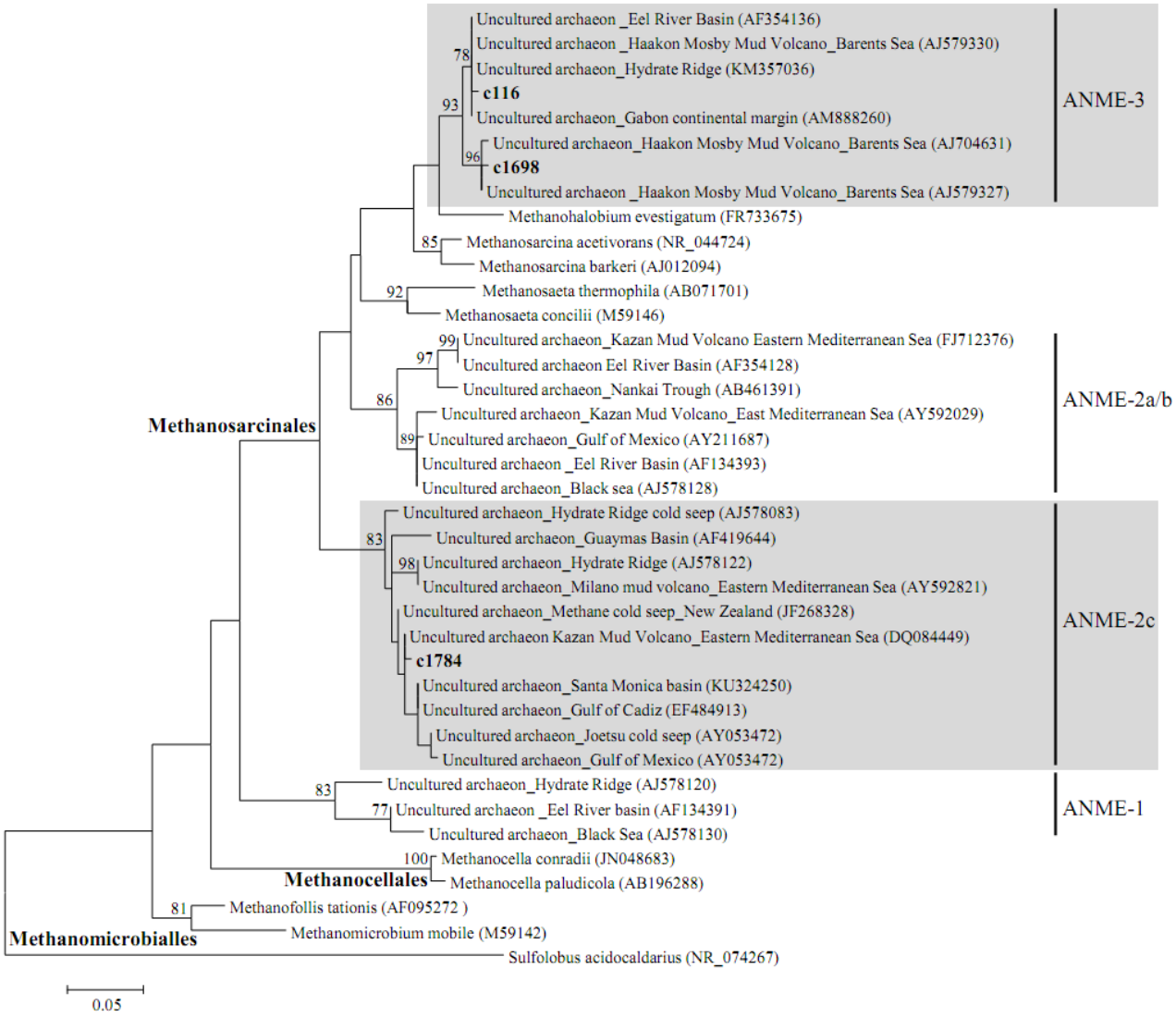
Uncultured archaeon _Eel River Basin (AF354136)
Uncultured archaeon _Haakon Mosby Mud Volcano_Barents Sea (AJ579330)
Uncultured archaeon_Hydrate Ridge (KM357036)
c116
Uncultured archaeon_Gabon continental margin (AM888260)
Uncultured archaeon_Haakon Mosby Mud Volcano_Barents Sea (AJ704631)
c1698
Uncultured archaeon _Haakon Mosby Mud Volcano_Barents Sea (AJ579327)
ANME-3
Methanohalobium evestigatum (FR733675)
Methanosarcina acetivorans (NR_044724)
Methanosarcina barkeri (AJ012094)
Methanosaeta thermophila (AB071701)
Methanosaeta concilii (M59146)
Uncultured archaeon_Kazan Mud Volcano Eastern Mediterranean Sea (FJ712376)
Uncultured archaeon Eel River Basin (AF354128)
Uncultured archaeon_Nankai Trough (AB461391)
Uncultured archaeon_Kazan Mud Volcano_East Mediterranean Sea (AY592029)
Uncultured archaeon_Gulf of Mexico (AY211687)
Uncultured archaeon _Eel River Basin (AF134393)
Uncultured archaeon_Black sea (AJ578128)
ANME-2a/b
Methanosarcinales
Uncultured archaeon_Hydrate Ridge cold seep (AJ578083)
Uncultured archaeon_Guaymas Basin (AF419644)
Uncultured archaeon_Hydrate Ridge (AJ578122)
Uncultured archaeon_Milano mud volcano_Eastern Mediterranean Sea (AY592821)
Uncultured archaeon_Methane cold seep_New Zealand (JF268328)
Uncultured archaeon Kazan Mud Volcano_Eastern Mediterranean Sea (DQ084449)
c1784
Uncultured archaeon_Santa Monica basin (KU324250)
Uncultured archaeon_Gulf of Cadiz (EF484913)
Uncultured archaeon_Joetsu cold seep (AY053472)
Uncultured archaeon_Gulf of Mexico (AY053472)
ANME-2c
Uncultured archaeon_Hydrate Ridge (AJ578120)
Uncultured archaeon _Eel River basin (AF134391)
Uncultured archaeon_Black Sea (AJ578130)
ANME-1
Methanocella conradii (JN048683)
Methanocella paludicola (AB196288)
Methanocellales
Methanofollis tationis (AF095272)
Methanomicrobium mobile (M59142)
Methanomicrobialles
Sulfolobus acidocaldarius (NR_074267)
78
93
96
85
92
99
97
86
89
83
98
83
77
100
81
0.05

Fig. 5